Bull. Mater. Sci. (2019) 42:231
https://doi.org/10.1007/s12034-019-1919-9

Modelling of novel-structured copper barium tin sulphide thin film solar cells

K YOUSAF HAMEED[1,2,*], B FAISAL[1,2], T HANAE[1,3], S BERNABÉ MARÍ[1], B SAIRA[4] and K NAVEED ALI KAIM[2]

[1]Schnool of Design Engineering, Universitat Politécnica de Valencia, Camí de Vera 46002, Spain
[2]Department of Electrical Engineering, Federal Urdu University of Arts, Science and Technology Islamabad, Islamabad 44000, Pakistan
[3]Laboratory Materials and Environment Engineering: Modeling and Application, University Ibn Tofail, Kenitra 14000, Morocco
[4]COMSATS University Islamabad, Islamabad 45550, Pakistan
*Author for correspondence (yousaf.hameedk@gmail.com)

MS received 17 October 2018; accepted 25 April 2019

Abstract. In this work, a novel structured Cu_2BaSnS_4 (CBTS)/ZnS/Zn(O, S) photovoltaic device is proposed. A nontoxic, earth-abundant and auspicious quaternary semiconductor compound copper barium tin sulphide (Cu_2BaSnS_4) is used as an absorber layer. We propose a novel Zn(O, S) buffer layer for a high-power conversion efficiency (PCE) of CBTS-based thin film photovoltaic cells. Solar cell capacitance simulator software is used for device modelling and simulations are performed under a 1.5 AM illumination spectrum. The proposed device is investigated by means of numerical modelling and optimized the parameters to maximize its efficiency. Promising optimized functional parameters had been achieved from the proposed structure with back surface field layer with a PCE of 18.18%, a fill factor of 83.45%, a short-circuit current of 16.13 mA cm^{-2} and an open-circuit voltage of 1.3 V. The promising results give an imperative standard for possible manufacturing of high efficiency, eco-friendly inorganic CBTS-based photovoltaic cells.

Keywords. Numerical analysis; SCAPS; photovoltaics; Cu_2BaSnS_4; CBTS; solar cell.

1. Introduction

The propitious choices to meet the growing demand in low-cost photovoltaic device fabrication is the use of air stable and earth-abundant materials [1,2]. Thin films' photoelectric power conversion efficiency (PCE) of conventional absorbers using copper indium gallium sulphide selenide (CIGSSe) and cadmium telluride (CdTe) solar cells reaches a conversion efficiency of 21.7 [3] and 21.5% [4], respectively. Since decades, a great effort has been achieved on the optimization of CIGSSe- and CdTe-based devices. The scalability of technology is limited for commercial use because of the rising cost and toxic nature of cadmium (Cd) content in the CdTe absorber and the scarcity of tellurium (Te), gallium (Ga) and indium (In) [5]. Recently, researchers have focussed their attention on the quaternary compound materials for the preparation of In- and Ga-free chalcogenide absorber materials [6]. The increasing demand of quaternary compounds for the fabrication of thin film solar cells is due to their potential [7–9]. Non-toxic earth-abundant quaternary compound materials, such as CZTS, CZTSe [10–13], CFTS, CFTSe [14], CBTS, CBTSe [1,15] and their alloys are emerging and promising replacement of chalcopyrite (CIGS, CIGSe) absorbers [16] by substituting low-cost contents, such as Ga with Sn and In with Zn or Ba in chalcopyrite absorbers [17–19]. Among quaternary compounds, Cu_2BaSnS_4 (CBTS) is one of the propitious compounds for an effective light absorber material due to its earth-abundant and nontoxic nature, suitable wide-optical band gap of 1.7–2.1 eV and large absorption coefficient, $\alpha > 10^4$ cm^{-1} [1,16,20]. In comparison with kesterite compounds, CBTS as a absorber is expected to serve as more efficient and better for photoelectrochemical and photovoltaic solar cells [21,22]. According to Shockley–Queisser limit, the maximum PCE of 22% using a AM 1.5 G spectrum is theoretically possible to conceive from a CBTS single junction solar cell and in the case of the tandem photovoltaic solar cell, if it is used in series with the silicon photovoltaic solar cell then, PCE will be boosted up to 34% [23]. In ref. [21], it is reported as the best device delivered a PCE of about 1.55%. The PCE of the CBTS solar cell of about 1.6% is presented in ref. [16]. The best PCE of about 2.03% was achieved from the proposed CBTS solar cell [1]. An experimentally conceivable PCE from the CBTS photovoltaic cell is still not as per SQ efficiency limit. It is just due to the lack of the understanding of material parameters. Numerical analysis is an important tool to better comprehend the material parameters. Thus, numerical modelling or numerical analysis plays a momentous role in the fabrication of high efficiency

Published online: 16 July 2019

photovoltaic cells [24]. We proposed the use of Zn(O, S) as a buffer layer for the CBTS thin film solar cell. It is an auspicious material due to its higher optical band gap and nontoxic nature that permits to collect the blue photons. The value of a conduction band offset (CBO) at the junction interface can be tuned by changing O and S contents of Zn(O, S) [25–27]. Our method for enhancing the efficiency and improving the performance of the CBTS-based photovoltaic device is due to the following facts:

- Validation of the CBTS experimental cell.
- Proposing novel structure of CBTS/ZnS/Zn(O, S)/FTO for solar cells.
- Proposing Zn(O, S) buffer layer for the CBTS solar cell.
- Optimization of absorber layer thickness and doping concentration.
- Optimization of stacked buffer layer thickness and doping concentration.
- Comparison of results.

Numerical modelling is an important tool for understanding the working parameters of the photovoltaic cell and it plays a momentous role in manufacturing of high efficiency photovoltaic devices [28]. For validation of the experimental reference cell, we take a solar cell structure from ref. [21] which was presented in our previous work [29]. Modelling of novel-structured CBTS is presented in this research. Solar cell capacitance simulator (SCAPS) software is used for investigation and device modelling [7]. The thickness of the CBTS absorber layer varies from 1 to 10 μm with a band gap energy of 1.9 eV. The band gaps of Zn(O, S)- and ZnS-stacked buffer layers are larger than those of the absorber layer. Therefore, in the CBTS layer, the photon absorption is maximum. The PCE and open-circuit voltage of a photovoltaic cell are improved due to these photon absorptions. The auspicious results of the proposed device will give valuable guidelines for researchers and engineers to manufacture a high-efficiency CBTS-based photovoltaic cell.

2. Numerical modelling and physical parameters

Device modelling can be performed by using the SCAPS software. SCAPS is designed for analysing energy bands, functional parameters (PCE, FF, J_{sc} and V_{oc}), spectral responses of a device, ac characteristics (C–V and C–f), J–V characteristics and doping concentration of materials by solving basic semiconductor equations [24]. For the better understanding of the photovoltaic device, device modelling software should solve the basic semiconductor equations such as Poisson and continuity equations. The Poisson equation is related to the electrostatic charge potential $\mathrm{div}(\varepsilon\nabla\Psi) = -\rho$, whereas the carrier continuity equation is related to holes and electrons (given in equations (1 and 2)) [30], where J_n and J_p are current densities.

$$\frac{\partial n}{\partial t} = \frac{1}{q}\,\mathrm{div}\,\overrightarrow{J_n} + G_n - R_n, \tag{1}$$

$$\frac{\partial p}{\partial t} = -\frac{1}{q}\,\mathrm{div}\,\overrightarrow{J_p} + G_p - R_p, \tag{2}$$

where p and n are hole and electron concentrations, J_p and J_n are hole and electron current densities, R_p and R_n are hole and electron recombination rates and G_p and G_n are hole and electron generation rates. Physical parameters such as absorber, window and buffer layer thicknesses, doping densities, intrinsic carrier concentrations, band gaps, electron affinities and electron–hole mobilities are used in SCAPS for device modelling. Physical parameters that are essential for device modelling are shown in table 1. The added values between the interface of p-CBTS/n-ZnS is $N_t = 1 \times 10^{15}$ (cm^{-2}) and the absorber layer is $N_t = 1 \times 10^{15}$ (cm^{-3}) are considered for validation purposes and given in table 1.

3. Result and discussion

3.1 *Validation of experimental results in SCAPS*

The functional parameters of the experimental solar cell presented in refs [21,29] were reproduced in SCAPS-1D software by adding absorber layer defects and absorber/buffer interface defects. Validation of the experimental device simulated in SCAPS was performed by using the p-CBTS/n-CdS interface defect value of $N_t = 1 \times 10^{15}$ (cm^{-2}) and the absorber layer defect value of $N_t = 1 \times 10^{15}$ (cm^{-3}). Device physical parameters and added defect densities used for SCAPS are given in tables 1 and 2, respectively. Functional parameters of the solar cell were PCE of 1.55%, V_{oc} of 0.63 V, J_{sc} of 5.25 mA cm^{-2} and FF of 66.71%. The experimental device J–V characteristic curve simulated in SCAPS is shown in figure 1.

3.2 *Device optimization*

The energy band diagram of the photovoltaic device structure CBTS/CdS/ZnO obtained from SCAPS is plotted in figure 2. The device properties can be explained well with the aid of the energy band diagram. From figure 2, it is clear that for the maximum light absorption, the optimal value of the band gap should be larger than or equivalent to the maximum value of the energy band gap, such as 1.9 eV.

Figure 3 shows the J–V characteristic of the CBTS/CdS/ZnO solar cell under light conditions after optimization of physical parameters like thickness and doping concentration of absorber and buffer layers. Device optimization gives the functional parameters such as PCE of 6.9%, V_{oc} of 0.78 V, J_{sc} of 11.64 mA cm^{-2} and FF of 74.77%.

This efficiency can further be improved by changing the band structure between the absorber and buffer layer. As explained in our previous work [35], the PCE of the solar cell is limited by an interface recombination between

Table 1. Device modelling of physical parameters used in SCAPS [1,16,31–34].

Material parameters	*p*-CBTS (absorber)	*n*-CdS (buffer)	*n*-ZnO (window)
Thickness, W (μm)	2	0.4	0.4
Band gap, E_g (eV)	1.9	2.45	3.3
Electron affinity, χ (eV)	3.6	4.4	4.5
Dielectric permittivity, ε_r	5.4	9	9
CB effective density of state, NC (cm^{-3})	2.2×10^{18}	1.8×10^{19}	2.2×10^{18}
VB effective density of state, NV (cm^{-3})	1.8×10^{19}	2.4×10^{18}	1.8×10^{19}
Electron–hole thermal velocity (cm^{-1})	$10^7/10^7$	$10^7/10^7$	$10^7/10^7$
Electron–hole mobilities, μ_e, μ_h ($cm^2V^{-1}\,s^{-1}$)	30/10	100/25	100/25
Electron and hole concentrations, n, p (cm^{-3})	1×10^{15}	5×10^{18}	1×10^{18}

Table 2. Added value of defects.

Properties	*p*-CBTS (absorber)	*p*-CBTS/*n*-CdS (interface)
Energy level with respect to reference (eV)	0.6	0.6
Total density, N_t	1×10^{15} cm^{-3}	1×10^{15} cm^{-2}
Capture cross-section area of electrons, δ_e (cm^2)	1×10^{-14}	2×10^{-15}
Capture cross-section area of holes, δ_h (cm^2)	1×10^{-14}	2×10^{-15}

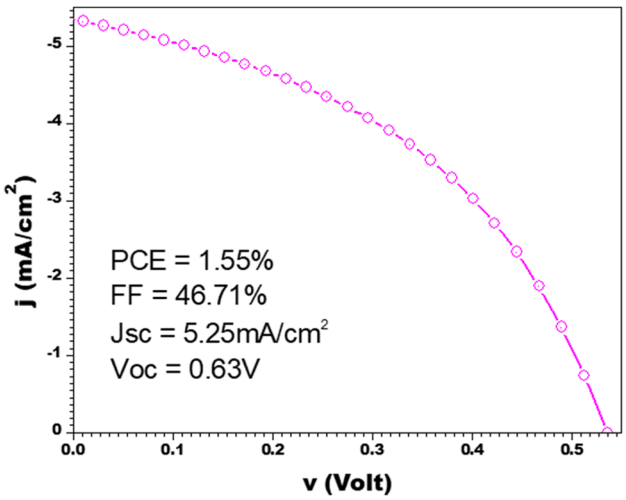

Figure 1. Experimental solar cell $J-V$ characteristics [21].

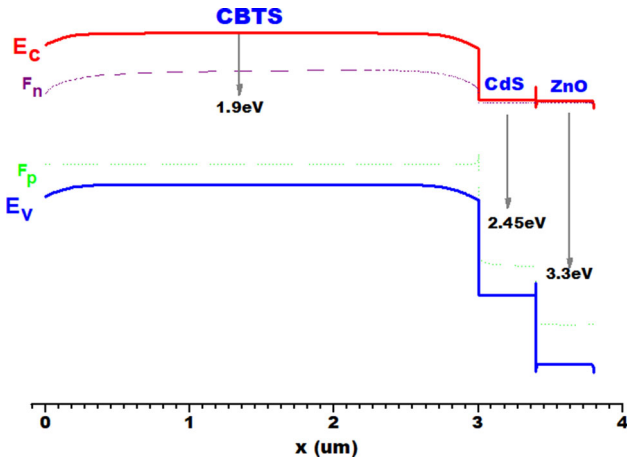

Figure 2. Energy band diagram.

the absorber/buffer interface. This recombination cannot be eliminated, but can be governed by changing the CBO between the absorber/buffer [14,35]. To analyse the effect of the CBO on the solar cell performance, an electron affinity (EA) of the buffer layer was varied from 4.4 to 3.3 eV. The results for the effect of EA on PCE and on interface recombination current of the solar cell are shown in figures 4 and 5. From figure 4, it is clear that with a decrease in the value of EA, there is an increase in PCE, whereas in figure 5, with a decrease in the value of EA, there is a decrease in the interface recombination current (J_{if_rec}) of the solar cell. This reduction in recombination current is the major reason for the efficiency enhancement of the optimized device.

From figures 4 and 5, the best results were achieved for the EA value of 3.4 eV and only material that is available in the literature having a EA of 3.4 eV with a band gap of 3.6 eV is ZnS [36]. So, to further enhance the PCE of this device, we change the structure of the device from CBTS/CdS/ZnO to CBTS/ZnS/Zn(O,S). In the next step, we further optimize the device performance of the CBTS/ZnS/ZnO structure.

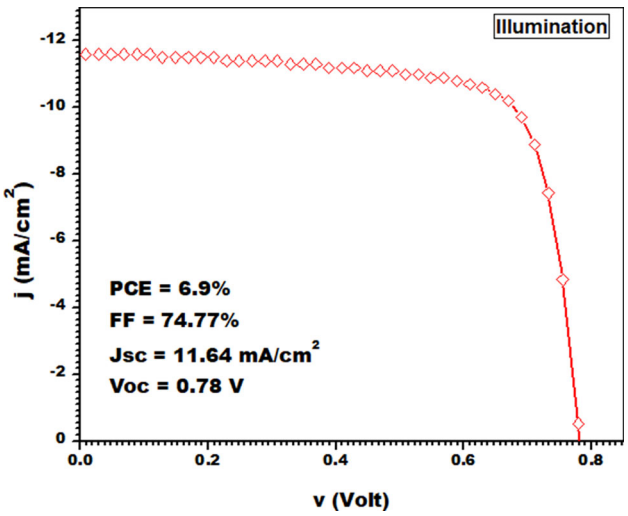

Figure 3. $J-V$ characteristics of the CBTS/CdS/ZnO solar cell.

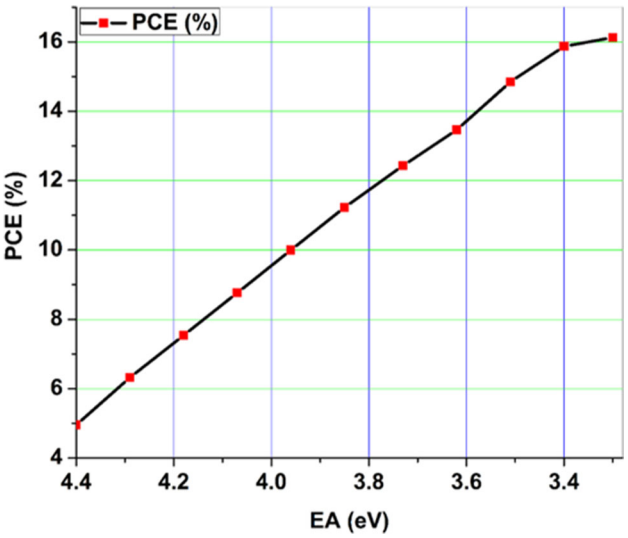

Figure 4. Effect of EA values on the PCE of the solar cell.

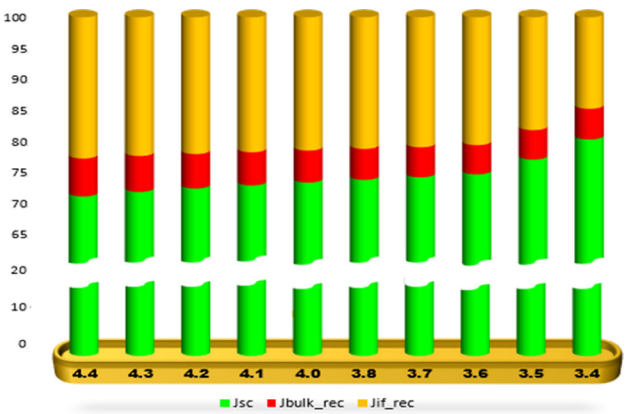

Figure 5. Effect of EA values on $J_{\text{if\_rec}}$ of the solar cell.

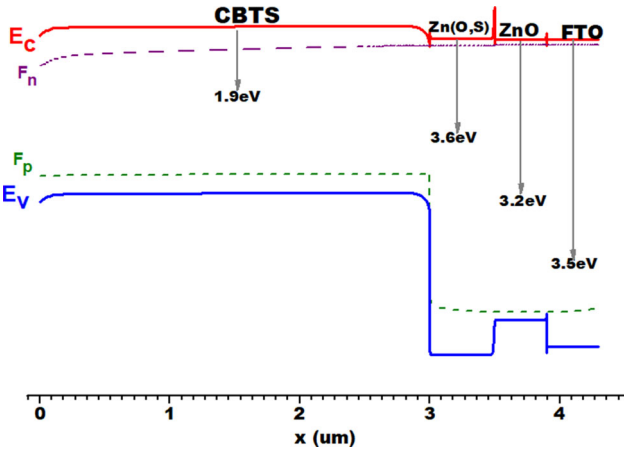

Figure 6. Energy band diagram of the proposed device.

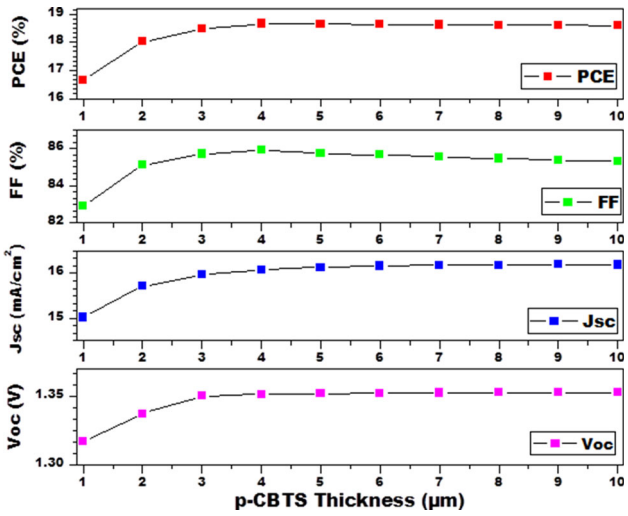

Figure 7. Absorber thickness effect.

3.3 *Proposed device energy band diagram and simulation parameters*

The energy band diagram of the proposed device structure (CBTS/ZnS/Zn(O, S)/FTO) of the solar cell is shown in figure 6 and is being taken from the SCAPS simulator to analyse the CBTS-based device. Physical parameters for the proposed device structure and added values of defects are given in tables 3 and 4, respectively. The energy band diagram explains the device properties. For the light absorption in the CBTS solar cell, the optimal value of the band gap energy should be larger than or equivalent to the maximum value of the energy band gap such as 1.9 eV.

The added values between the interface of p-CBTS/n-ZnS is $N_t = 1 \times 10^{15}$ (cm^{-2}) and the absorber layer is $N_t = 1 \times 10^{15}$ (cm^{-3}) are considered for validation purposes.

Table 3. Physical parameters used in SCAPS for proposed device modelling [1,14,16,31–34,36].

Material parameters	*p*-CBTS (absorber)	*n*-ZnS (buffer-1)	*n*-Zn (O, S) (buffer-2)	*n*-FTO (window)
Thickness, W (μm)	2	0.4	0.4	0.5
Band gap, E_g (eV)	1.9	2.45	3.3	3.5
Electron affinity, χ (eV)	3.6	4.4	4.5	4
Dielectric permittivity, ε_r	5.4	9	9	9
CB effective density of state, NC (cm^{-3})	2.2×10^{18}	1.8×10^{19}	2.2×10^{18}	1×10^{19}
VB effective density of state, NV (cm^{-3})	1.8×10^{19}	2.4×10^{18}	1.8×10^{19}	1×10^{18}
Electron–hole thermal velocity (cm^{-1})	$10^7/10^7$	$10^7/10^7$	$10^7/10^7$	$10^7/10^7$
Electron–hole mobilities, μ_e, μ_h ($cm^2\ V^{-1}\ s^{-1}$)	30/10	100/25	100/25	20/10
Electron and hole concentrations, n, p (cm^{-3})	1×10^{15}	5×10^{18}	1×10^{18}	1×10^{18}

Table 4. Added value of defects.

Properties	*p*-CBTS/*n*-ZnS (interface)	*p*-CBTS (absorber)
Energy level with respect to reference (eV)	0.6	0.6
Total density, N_t	$1 \times 10^{15}\ cm^{-2}$	$1 \times 10^{15}\ cm^{-3}$
Capture cross-section area of electrons, δ_e (cm^2)	1×10^{-15}	1×10^{-14}
Capture cross-section area of holes, δ_h (cm^2)	1×10^{-15}	1×10^{-14}

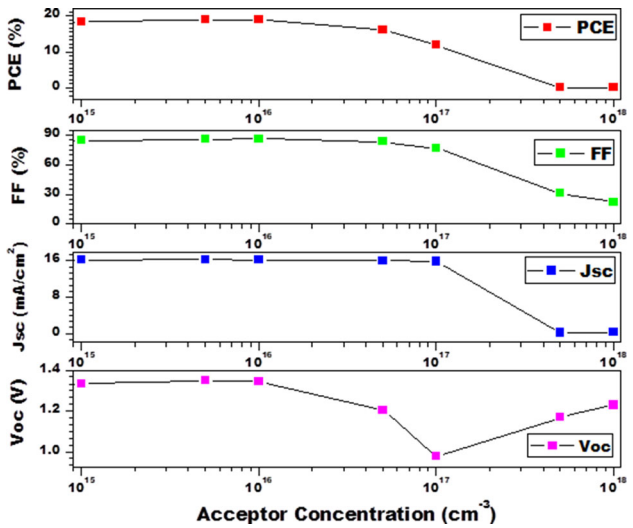

Figure 8. Absorber doping concentration effect.

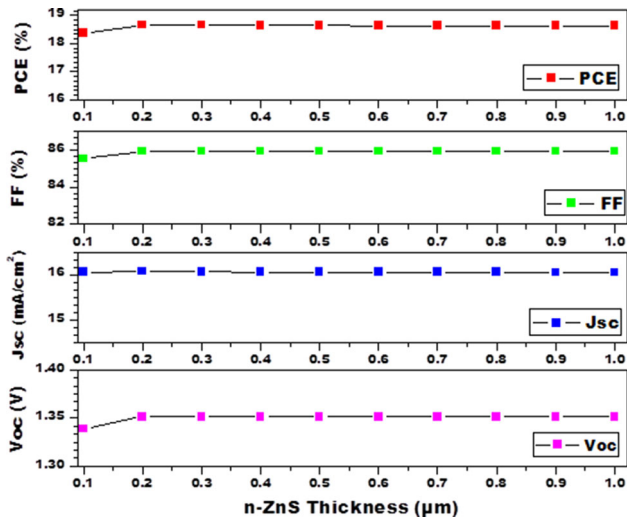

Figure 9. ZnS thickness effect.

3.4 *CBTS layer thickness and doping concentration effect on device performance*

Functional parameters of the CBTS photovoltaic cell are affected by changing the absorber thickness. The PCE increases with an increase in the absorber thickness value. Functional parameters affected due to the change in the absorber thickness are illustrated in figure 7. The solar cell performance is examined by changing the absorber thickness value from 1 to 10 μm. The other different layer material parameters are kept constant. All functional parameters such as PCE, FF, J_{sc} and V_{oc} are initially increased with an increase in the absorber thickness. This increase in functional parameters is up to an optimum absorber thickness and predominantly, increase in J_{sc} with an increase in V_{oc} and PCE is due to the photon absorption energy of longer

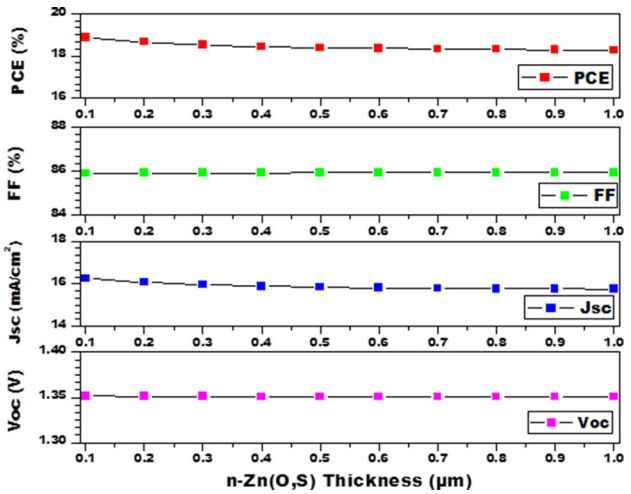

Figure 10. Zn(O, S) buffer thickness effect.

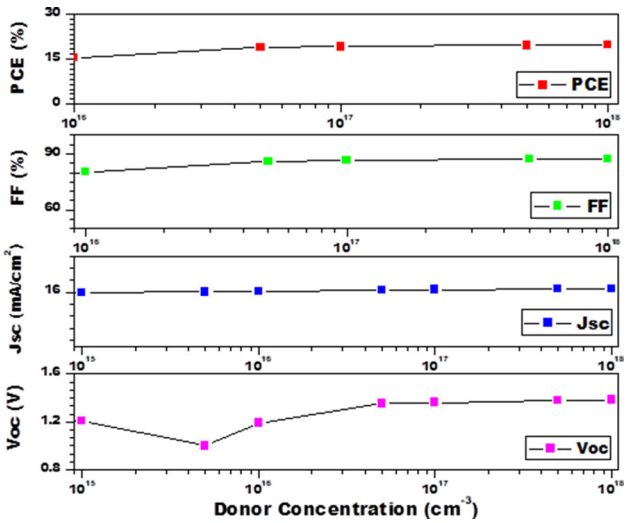

Figure 11. ZnS buffer layer donor concentration effect.

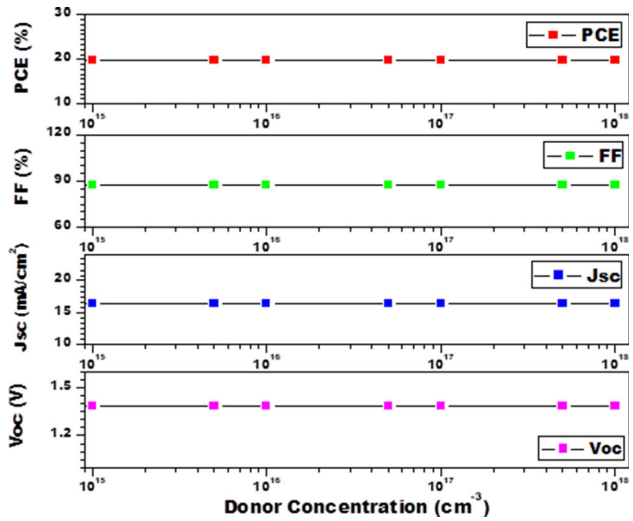

Figure 12. Zn(O, S) buffer layer donor concentration effect.

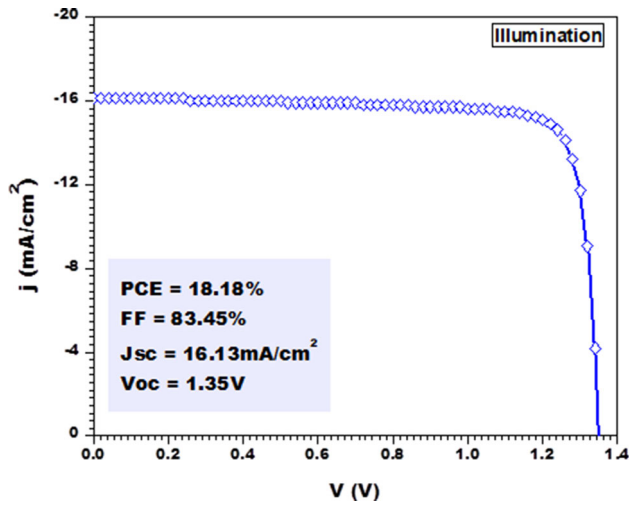

Figure 13. J–V characteristics under light illumination.

wavelengths and the ratio of photogenerated carriers. After the optimum absorber thickness value, PCE and J_{sc} remain constant, whereas very small decrease is found in FF and V_{oc}. The optimal absorber width for the proposed device is 4 μm.

Effects of an acceptor doping concentration on the functional parameters are also analysed to assess the device performance. The doping concentration effect on the CBTS-based photovoltaic cell performance can be shown in figure 8. The acceptor doping concentration of the absorber layer varies from 1×10^{15} to 1×10^{19} cm^{-3}. Figure 8 illustrates that initially all functional parameters have constant values. The proposed device has the optimal acceptor doping concentration value of about 5×10^{15} cm^{-3}. In figure 8, if there is a further increase in the doping concentration value, all functional parameters start to decrease. After reaching 1×10^{17} cm^{-3}, V_{oc} again starts to increase, whereas the other functional parameters, such as PCE, FF and J_{sc} remain constant. Higher carrier densities are the reason for the decrease in the value of J_{sc}, due to this, the recombination process rises and photon-generated electron collection probability reduces. The collected PCE of the CBTS-based solar cell is more dependent on this analysed factor.

3.5 *Stacked buffer layer thickness and doping concentration effect on device performance*

Effects of ZnS and Zn(O, S)-stacked buffer layers on the performance of the CBTS photovoltaic cell are also explored in this analysis and are shown in figures 9 and 10, respectively. In both cases, buffer layer thicknesses are varying from 0.1 to 1 μm. Simulated fallout shows that no change was found in functional parameters with an increase in the buffer thickness. So, this result is comprehended that an increase

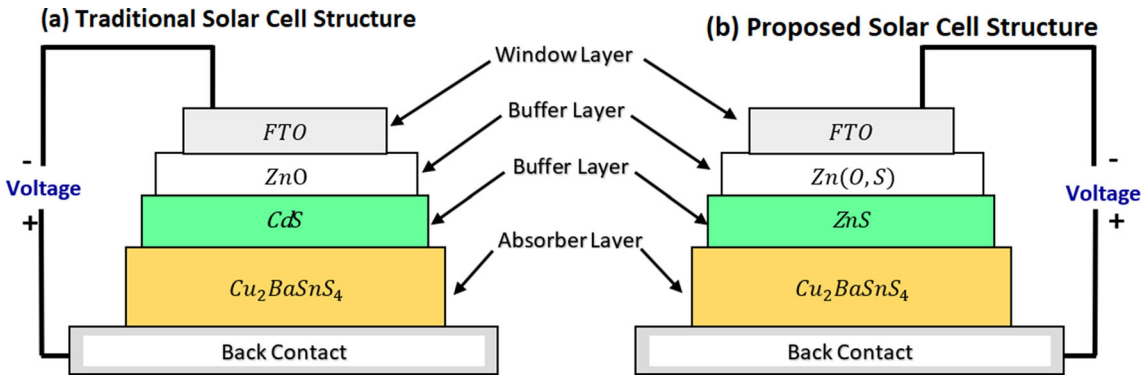

Figure 14. Device structure comparison of the proposed and traditional solar cells.

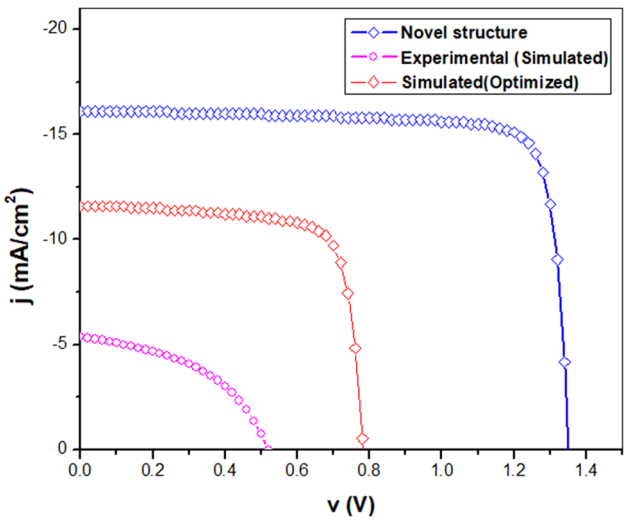

Figure 15. $J-V$ characteristics of curve comparison.

in both buffer layer thicknesses not affects the device performance. For designing the CBTS/ZnS/Zn(O, S) solar cell, the optimum thickness taken for ZnS is 0.2 μm and for Zn(O, S) is 0.1 μm.

The impact of the donor doping concentration on the proposed device performance is also explored in this numerical modelling. Simulated fallouts of the stacked-buffer layers, such as ZnS and Zn(O, S) are shown in figures 11 and 12, respectively. In both cases, the doping concentration densities vary from 1×10^{15} to 1×10^{18} cm^{-3}. Figure 11 illustrates an increase in the donor doping concentration of the ZnS buffer layer, there is no variation found in PCE, FF and J_{sc}. Initially, V_{oc} decreases up to the optical value of the donor concentration value, but after that, it will start to increase as shown in figure 11. The reason behind this is when the value of the donor concentration increases from the value of the acceptor concentration; the interface recombination is totally governed by the majority of electrons and no holes are present for recombination. So, deficit in V_{oc} is recovered when N_d exceeds the value of N_a. From figure 8, the optimum value of the donor concentration of the ZnS buffer layer is 1×10^{18} cm^{-3}.

Figure 12 shows that functional parameters of the proposed device are not deviated with an increase in the doping concentration of Zn(O, S). So, the result is comprehended that variation in donor concentration density of Zn(O, S) is not affected the performance of the proposed device. The optimum value of the donor concentration of the Zn(O, S) buffer layer taken is 1×10^{18} cm^{-3}.

3.6 *J–V characteristics of proposed device structure*

The photovoltaic cell converts the light radiation energy into electrical energy. Under light conditions, the photovoltaic cell starts working. Photogenerated carriers are the main cause of the flow of current through the device. Figure 13 shows the $J-V$ characteristic of the proposed CBTS/ZnS/Zn (O, S) / FTO device. Device optimization gives the PCE of 18.18%, FF of 83.45%, V_{oc} of 1.35 V and J_{sc} of 16.13 mA cm^{-2} by optimizing the device physical parameters, such as an acceptor doping concentration of 5×10^{15} cm^{-3} and a absorber thickness of 2 μm.

3.7 *Result comparison*

The comparison of $J-V$ characteristics curves of the experimental device with the optimized solar cell and novel proposed structure is shown in figures 14 and 15. Figure 15 shows the improved results of a novel structure in comparison with the referenced solar cell.

Table 5 presents the comparison of functional parameters (PCE, FF, J_{sc} and V_{oc}) of the experimental solar cell with its optimized parameters and novel proposed structure device. All the improved parameters are given in table 5. In this work, the promising results had been achieved with a conversion efficiency of 18.18%, FF of 83.45%, J_{sc} of 16.13 mA cm^{-2} and V_{oc} of 1.35 V.

Table 5. Comparison of functional parameters.

	PCE (%)	FF (%)	J_{sc} (mA cm^{-2})	V_{oc} (V)
SCAPS simulated experimental device	1.56	47.12	5.1	0.64
Simulated (optimized)	6.9	74.77	11.64	0.78
Proposed device	18.18	83.45	16.13	1.35

4. Conclusions

A novel structure for the CBTS-based device CBTS/ZnS/Zn(O, S)/FTO is proposed in this work. SCAPS simulation software is used for the modelling and analysing the CBTS-based photovoltaic cell. Essential parameters like thicknesses and doping concentrations of absorber and stacked buffer layers are analysed. This work will provide the necessary guidelines for analysing and fabricating high efficiency CBTS-based solar cells. The promising results had been achieved with a PCE of 18.18%, FF of 83.45%, J_{sc} of 16.13 mA cm^{-2} and V_{oc} of 1.35 V. The results proposed in this work will play a significant role and gives an imperative standard for the possible production of eco-friendly and high efficiency inorganic CBTS-based photovoltaic cells.

Acknowledgements

This work was supported by Ministerio de Economía y Competitividad (ENE2016-77798-C4-2-R) and Generalitat valenciana (Prometeus 2014/044).

References

[1] Ge J, Koirala P, Grice C R, Roland P J, Yu Y, Tan X *et al* 2017 *Adv. Energy Mater.* **7** 1601803
[2] Khattak Y H, Mahmood T, Alam K, Sarwar T, Ullah I and Ullah H 2014 *Am. J. Electr. Power Energy Syst.* **3** 86
[3] Steinmann V, Brandt R E and Buonassisi T 2015 *Nat. Photonics* **9** 355
[4] Jackson P, Hariskos D, Wuerz R, Kiowski O, Bauer A, Friedlmeier T M *et al* 2015 *Phys. Status Solidi: Rapid. Res. Lett.* **9** 28
[5] Shin D, Saparov B and Mitzi D B 2017 *Adv. Energy Mater.* **7** 1602366
[6] Paper C, Le A, Universit D, Universit B, Universit M A, Marchionna S *et al* 2017 *Eur. Photovolt. Sol. Energy Conf.* **33** 25
[7] Khattak Y H, Baig F, Ullah S, Marí B, Beg S and Ullah H 2018 *J. Renew. Sustain. Energy* **10** 033501
[8] Fontané X, Izquierdo-Roca V, Saucedo E, Schorr S, Yukhymchuk V O, Valak M Y *et al* 2012 *J. Alloys Compd.* **539** 190
[9] Zhang X, Bao N, Ramasamy K, Wang Y-H A, Yifeng Wang B L and Gupta A 2012 *Chem. Commun.* **48** 4956
[10] Adewoyin A D, Olopade M A and Chendo M 2017 *Optik—Int. J. Light Electron Opt.* **133** 122
[11] Boutebakh F Z, Zeggar M L, Attaf N and Aida M S 2017 *Optik—Int. J. Light Electron Opt.* **144** 180
[12] Ananthakumar S, Ram Kumar J and Moorthy Babu S 2016 *Optik—Int. J. Light Electron Opt.* **127** 10360
[13] Jianjun L, Dongxiao W, Xiuling L and Zeng Y 2018 *Adv. Sci.* **5** 1700744
[14] Khattak Y H, Baig F, Ullah S, Marí B, Beg S and Ullah H 2018 *Optik—Int. J. Light Electron Opt.* **164** 547
[15] Xiao Z, Meng W, Li J V. and Yan Y 2017 *ACS Energy Lett.* **2** 29
[16] Shin D, Saparov B, Zhu T, Huhn W P, Blum V and Mitzi D B 2016 *Chem. Mater.* **28** 477
[17] Repins I L, Romero M J, Li J V, Wei S-H, Kuciauskas D, Jiang C-S *et al* 2013 *J. Photovoltaics* **3** 439
[18] Zhou H, Hsu W-C, Duan H-S, Bob B, Yang W, Song T-B *et al* 2013 *Energy Environ. Sci.* **6** 2822
[19] Khattak Y H, Baig F, Toura H, Ullah S, Marí B, Beg S *et al* 2018 *Curr. Appl. Phys.* **18** 633
[20] Ge J, Roland P J, Koirala P, Meng W, Young J L, Petersen R *et al* 2017 *Chem. Mater.* **29** 916
[21] Ge J and Yan Y 2017 *J. Mater. Chem. C* **5** 6406
[22] Hong F, Lin W, Meng W and Yan Y 2016 *Phys. Chem. Chem. Phys.* **18** 4828
[23] Todorov T, Gunawan O and Guha S 2016 *Mol. Syst. Des. Eng.* **1** 370
[24] Baig F, Ullah H, Khattak Y H and Mari Soucase B 2016 *Int. Ren. Sus. En. Conf.* 596, https://doi.org/10.1109/IRSEC.2016.7983899
[25] Lin L-Y, Qiu Y, Zhang Y and Zhang H 2016 *Chinese Phys. Lett.* **33** 10780
[26] Platzer B C, Törndahl T, Abou-Ras D, Malmström J, Kessler J and Stolt L 2006 *J. Appl. Phys.* **100** 044506
[27] Persson C, Platzer-Björkman C, Malmström J, Törndahl T and Edoff M 2006 *Phys. Rev. Lett.* **97** 146403
[28] Burgelman M, Nollet P and Degrave S 2000 *Thin Solid Films* **361** 527
[29] Khattak Y H, Baig F, Soucase B M and Beg S 2018 *Mater. Focus* **84** 758
[30] Simya O K, Mahaboobbatcha A and Balachander K A 2015 *Superlattices Microstruct.* **82** 248
[31] Shin D, Zhu T, Huang X, Gunawan O, Blum V and Mitzi D B 2017 *Adv. Mater.* **29** 1
[32] Saha U and Alam M K 2018 *Phys. Status Solidi: Rapid Res. Lett.* **12** 1
[33] Zhu T, Huhn W P, Wessler G C, Shin D, Saparov B, Mitzi D B *et al* 2017 *Chem. Mater.* **29** 7868
[34] Ge J, Grice C R and Yan Y 2017 *J. Mater. Chem. A* **5** 2920
[35] Baig F, Khattak Y H, Marí B, Beg S, Gillani S R and Ahmed A 2018 *Optik—Int. J. Light Electron Opt.* **170** 463
[36] Khattak Y H, Baig F, Ullah S, Marí B, Beg S and Gillani S R 2018 *Optik—Int. J. Light Electron Opt.* **171** 453